(1)

A Rescaling Algorithm for the Numerical Calculation of Blowing-up Solutions

MARSHA BERGER AND ROBERT V. KOHN
Courant Institute

1. Introduction

We present a numerical study of the blow-up of $u_t = u_{xx} + u^p$. This is one of a large class of nonlinear evolution equations with scale-invariant structure and blowing-up solutions. Other examples include reaction diffusion equations such as $u_t - \Delta u = u^p$ or $u_t - \Delta u = e^u$, which arise in models of combustion (e.g. [21], [22]), and the nonlinear Schrödinger equation $iu_t - \Delta u = |u|^{p-1}u$, which arises in plasma physics and nonlinear optics (e.g. [24], [25]). The blowing-up solutions of such equations have in common the properties that (i) the singularities are isolated, and (ii) the singularities have a characteristic structure, which may or may not be directly linked to the scaling properties of the equation. For solutions that do develop singularities it is often of interest to study the local features of the blow-up. Such a study may be useful not only for direct comparison to the phenomenon being modelled, but also for extending the solution beyond the singular time, or for matching it to the solution of a different equation which applies near the singularity.

Several authors have attempted to calculate the local character of the blow-up of $u_t = u_{xx} + u^p$ numerically (e.g. [6], [13], [20]). This is a sensitive problem, since most methods for solving evolution equations lose accuracy as the solution becomes large. Two novel approaches have recently been introduced, in somewhat different contexts: Chorin used an algorithm based on rescaling and mesh refinement to study the three-dimensional Euler and Navier-Stokes equations in [7]; and a method based on continuous-in-time rescaling has been applied by LeMesurier, McLaughlin, Papanicolaou, P.-L. Sulem, and C. Sulem to study the nonlinear Schrödinger equation in [24], [25].

Our approach differs from those just cited in the following way. Upon rescaling to resolve the appearing singularity, Chorin's method concentrates on an increasingly small physical domain, enforcing periodic boundary conditions closer and closer (in unscaled distance) to the singularity. The method of LeMesurier et al. uses a fixed mesh in physical space which is spread apart by rescaling, so that accuracy is inevitably lost far from the singularity. In contrast, using our mesh refinement strategy we are able to compute accurately over the entire physical interval even as the solution grows in magnitude from $O(1)$ to $O(10^{12})$. The main idea is this: we step the solution forward until its maximum value reaches a preset threshold. Where the resulting function is large the solution is rescaled to make it small again. Since scaling stretches the spatial

Communications on Pure and Applied Mathematics, Vol. XLI, 841–863 (1988)

CCC 0010-3640/88/060841-23$04.00

variable, extra grid points are added to maintain accuracy. The rescaled solution is then stepped forward until its maximum value reaches the threshold value, at which juncture a further rescaling takes place, etc. In effect, our procedure solves the equation with a varying mesh width and time step that are linked, at each point in space-time, to the magnitude of the solution. Though very similar to Chorin's method in spirit, ours has the advantage that the boundary conditions for the rescaled problems are handled in a manner that is consistent with the underlying evolution equation. Our approach to mesh refinement and multiple grids is similar to one which has been used for solving first-order hyperbolic systems in one or more space dimensions; see e.g. [4]. In fact, we implemented the algorithm by modifying a code originally developed to solve hyperbolic systems in one space dimension.

Though the method is obviously more general, we have applied it only to the semilinear heat equation

$$u_t = u_{xx} + u^p, \qquad p > 1, \tag{1.1}$$

on the interval $-1 < x < 1$, with a Dirichlet boundary condition $u(-1, t) = u(1, t) = 0$. Attention is further restricted to initial data $\phi(x)$ such that

$$\phi > 0, \quad \phi(x) = \phi(-x), \quad x\frac{d\phi}{dx} < 0 \quad \text{for} \quad x \neq 0, \tag{1.2}$$

for which the solution of (1.1) is positive, symmetric, and radially decreasing. A lot is known about how solutions of this equation blow up; see e.g. [1], [2], [5], [10]–[19], [23], [26]. In particular, one knows that

$$\lim_{t \uparrow T} (T - t)^{1/(p-1)} u(\xi\sqrt{T-t}, t) = (p-1)^{-1/(p-1)} \tag{1.3}$$

uniformly for $|\xi| < C$, where T is the blow-up time; see [14], [16]. This gives the behavior in any space-time parabola $|x|^2 < C(T-t)$ based at the blow-up point. It is natural to ask what happens beyond these parabolas. For example, what is the asymptotic shape of the curve where $(T-t)^{1/(p-1)}u$ is constant?

In [13], [14], Galaktionov and Posashkov use a formal argument adapted from [20] to derive the ansatz

$$u(x, t) \sim (T-t)^{\frac{-1}{p-1}} \left[(p-1) + \frac{(p-1)^2}{4p} \frac{x^2}{(T-t)|\log(T-t)|} \right]^{\frac{-1}{p-1}}. \tag{1.4}$$

This is consistent with (1.3), since the second term in the bracket tends to zero as $t \to T$ with $\xi = x/\sqrt{T-t}$ fixed. It suggests that the curves $(T-t)^{1/(p-1)}u = \gamma$ are asymptotically of the form $x^2 = c(\gamma)(T-t)|\log(T-t)|$. (An analogous conjecture concerning the blow-up of $u_t - u_{xx} = e^u$ is presented in [9].) Some preliminary analytical results tending to confirm (1.4) are given in [10] and [14], but they fall far short of a full proof. Our numerical calculations give sufficient detail of the behavior near blow-up to allow us to test (1.4). The calculated solution is in fact in excellent agreement with the formula, leaving little doubt in our minds about the validity of this conjecture.

2. The Algorithm

The basis of our algorithm is the following scale invariance of the equation (1.1): if $u(x, t)$ solves it, then so does

$$u_\gamma(y, \tau) = \gamma^{2/(p-1)} u(\gamma y, \gamma^2 \tau) \tag{2.1}$$

for any $\gamma > 0$. By choosing γ to be small when u is large, one can keep the rescaled solution u_γ bounded. Thus it is easier to solve for u_γ than it is to compute u directly. Note however that both space and time are stretched by the scaling: if u is defined for $-1 < x < 1$ and $0 < t < T$, then the domain of u_γ is $-\gamma^{-1} < y < \gamma^{-1}$, $0 < \tau < \gamma^{-2}T$. This is the price one pays for the advantages of rescaling. Computationally, if u is defined on a grid of mesh width Δx, then (2.1) defines u_γ only on a grid of mesh width $\gamma^{-1}\Delta x$. A loss of accuracy is avoided by introducing additional points to the grid on which u_γ is defined. Our algorithm maintains both the original u and the rescaled u_γ, each defined on a separate grid, and steps each forward in a time-accurate way. Since the scaling (2.1) stretches time as well as space, most of the computational effort goes into the advancing of u_γ. Actually, our algorithm has an iterative structure, so that at the k-th iteration we are maintaining not just one rescaled solution but k of them, corresponding to $\gamma = \lambda, \lambda^2, \cdots, \lambda^k$, where λ is a fixed scaling parameter. To avoid unnecessary computation we rescale only where u is large, in such a way that the finest rescaled solution (u_γ with $\gamma = \lambda^k$ in the k iteration) stays bounded away from 0 as well as ∞.

To determine the algorithm one must fix three parameters:

$$\begin{aligned} \lambda &= \text{scale factor,} \\ M &= \text{maximum height before rescaling,} \\ \alpha &= \text{parameter controlling width of the interval to be rescaled} \\ &\quad \text{(which is where } \alpha M \leqq u \leqq M\text{).} \end{aligned} \tag{2.2}$$

They should be chosen so that

$$\lambda^{-1} > 1 \text{ is a small integer, and } 0 < \alpha < 1. \tag{2.3}$$

Typical choices are $\lambda = \frac{1}{4}$, $M = 2\sqrt{2}$, $\alpha = \frac{1}{2}$. The algorithm computes successively a sequence of functions $u_k(y_k, \tau_k)$, where

$$
\begin{aligned}
&u_k = k\text{-th rescaled solution},\\
(2.4)\qquad &y_k = k\text{-th rescaled spatial variable},\\
&\tau_k = \text{clock measuring (rescaled) time for } u_k.
\end{aligned}
$$

The time (according to the clock τ_k) at which u_k is rescaled to yield u_{k+1} will be denoted by τ_k^*, and the interval which is rescaled will be (y_k^-, y_k^+). All these quantities will be defined more precisely below. The initial index $k = 0$ corresponds to the "real" solution u as a function of "real" space x and "real" time t:

$$(2.5)\qquad u_0 = u, \quad y_0 = x, \quad \tau_0 = t.$$

The initial phase of the algorithm simply integrates the equation (1.1) until the maximum amplitude reaches M. (We assume that the initial data ϕ satisfy $\phi \leqq M$, and that the corresponding solution u does indeed blow up. This is true, for example, if $\phi = c(1 + \cos(\pi x))$ with c sufficiently large, and $M > 2c$.) We use the forward Euler finite difference scheme

$$
\begin{aligned}
&u(x_j, t_{n+1}) = u(x_j, t_n)\\
(2.6)\qquad &+\frac{\Delta t}{(\Delta x)^2}\left[u(x_{j-1}, t_n) - 2u(x_j, t_n) + u(x_{j+1}, t_n)\right] + \Delta t \cdot u^p(x_j, t_n),
\end{aligned}
$$

which is first-order accurate in time and second-order in space. Typical choices are $\Delta x = .005$ and $\Delta t = \frac{1}{4}(\Delta x)^2$. In this initial phase of the algorithm the Dirichlet condition $u = 0$ is used at the endpoints $x = \pm 1$. The solution is integrated until the first time step when $\|u(\cdot, t_n)\|_\infty > M$. Then it is linearly interpolated in time, using two time levels, to obtain a time τ_0^* with $t_n - \Delta t \leqq \tau_0^* \leqq t_n$ such that

$$(2.7)\qquad \|u(\cdot, \tau_0^*)\|_\infty = M.$$

The interval to be rescaled at the next stage, (y_0^-, y_0^+), is essentially the set where $u(\cdot, \tau_0^*) \geqq \alpha M$. It is convenient however to let $y_0^\pm$ be grid points, so they are defined by

$$
\begin{aligned}
&u(y_0^- - \Delta x, \tau_0^*) < \alpha M \leqq u(y_0^-, \tau_0^*),\\
(2.8)\qquad &u(y_0^+, \tau_0^*) \geqq \alpha M > u(y_0^+ + \Delta x, \tau_0^*).
\end{aligned}
$$

Of course, perfect arithmetic would yield $y_0^- = -y_0^+$. We do not enforce this

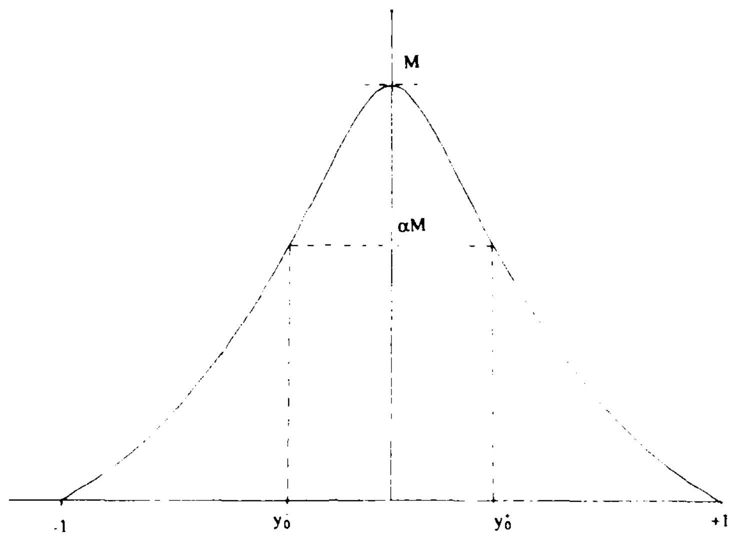

Figure 1. The graph of u_0 just prior to rescaling.

condition, so that symmetry may be used as an indicator of the accuracy of the computation. Figure 1 depicts the graph of u at the end of this initial phase, just prior to rescaling.

The first "rescaled solution" u_1 is related to u by

$$u_1(y_1, \tau_1) = \lambda^{2/(p-1)} u(\lambda y_1, \tau_0^* + \lambda^2 \tau_1). \tag{2.9}$$

We want u to be evaluated on the right of (2.9) only where $u \geqq \alpha M$; therefore y_1 is restricted to the interval

$$\lambda^{-1} y_0 \leqq y_1 \leqq \lambda^{-1} y_0^* . \tag{2.10}$$

The maximum value of u_1 at its initial time $\tau_1 = 0$ (corresponding to $t = \tau_0^*$) is reduced from $M = \|u(\cdot, \tau_0^*)\|_\infty$ to

$$\|u_1(\cdot, 0)\|_\infty = \lambda^{2/(p-1)} M < M;$$

this is the purpose of rescaling. Due to the scale invariance property (2.1), u_1 solves the *same* equation as u, with respect to *its* (rescaled) "space" and "time" variables $y_1 = x/\lambda$, $\tau_1 = (t - \tau_0^*)/\lambda^2$:

$$\frac{\partial}{\partial \tau_1} u_1 - \frac{\partial^2}{\partial y_1^2} u_1 = u_1^p . \tag{2.11}$$

This is what lies at the foundation of our algorithm: the difference scheme (2.6) originally introduced for stepping $u = u_0$ forward in time can also be used to solve for u_1 (and, eventually, for each successive u_k).

The computation of u_1 requires initial data $u_1(\cdot, 0)$ and boundary data $u_1(\lambda^{-1}y_0^{\pm}, \tau_1)$. The former are obtained by rescaling u:

$$u_1(y_1, 0) = \lambda^{2/(p-1)}u(\lambda y_1, \tau_0^*). \tag{2.12a}$$

The latter are obtained using the coarse mesh approximation method (see [8]): the boundary condition for the refined problem is determined by the solution previously computed in the same region using the coarser mesh. Specifically, the right side of equation

$$u_1(\lambda^{-1}y_0^{\pm}, N\Delta\tau_1) = \lambda^{2/(p-1)}u(y_0^{\pm}, \tau_0^* + \lambda^2 N\Delta\tau_1) \tag{2.12b}$$

is obtained by applying the forward Euler difference scheme to u with a time step $\lambda^2\Delta\tau_1$ (which is smaller than the full time step $\Delta\tau_0 = \Delta t$ used to advance u on the coarse mesh), but only at the points $y_0^{\pm}$ (which were chosen to be grid points). For first-order difference approximations in time, this is equivalent to linear interpolation in time between $u(y_0^{\pm}, t_n)$ and $u(y_0^{\pm}, t_n + \Delta t)$. Since the mesh ratio $\Delta\tau_1/(\Delta y_1)^2$ is stable (see below), we expect a boundary condition obtained via the coarse mesh approximation using a smaller time step to be stable as well. Such a result has been proved in other contexts, e.g. [3].

As has already been indicated, the "rescaled solution" u_1 is computed using the forward Euler scheme in the variables y_1, τ_1. To preserve the numerical scheme and to maintain accuracy, it is important to use the same discretization for u_1 as for u, i.e., to set $\Delta y_1 = \Delta x$ and $\Delta\tau_1 = \Delta t$. This requires introducing new grid points: those used for u, spaced Δx apart, determine $u_1(\cdot, 0)$ only on a mesh of width $\lambda^{-1}\Delta x$. To achieve $\Delta y_1 = \Delta x$, $\lambda^{-1} - 1$ new points must be introduced between each pair of existing ones. (If for example $\lambda = \frac{1}{4}$, then 3 new points are added to each interval to refine the mesh from $4\Delta x$ to Δx. The condition that λ^{-1} be a smaller integer is imposed to make this step easy to implement.) Linear interpolation in space is used to assign a value to $u_1(\cdot, 0)$ at the new grid points. Notice that the effect of this procedure in the original variable x is to refine the mesh by a factor of λ^{-1}.

The structure of our algorithm should now be clear: after rescaling, the "original" solution u and the "rescaled" solution u_1 are stepped forward independently, each on its own grid. A single time step of u corresponds to λ^{-2} time steps of u_1. The two solutions interact primarily in that u is used to determine the boundary conditions for u_1. In addition, at each successive time step for u the coarse grid solution is modified on the interval that was rescaled, to make it agree with the more accurate fine grid solution u_1. When $\|u_1(\cdot, N\Delta\tau_1)\|_\infty$ first exceeds M, a smaller time step (equivalently, linear interpolation in time) is used to find a value τ_1^*, with $(N-1)\Delta\tau_1 \leqq \tau_1^* \leqq N\Delta\tau_1$ such that

$$\|u_1(\cdot, \tau_1^*)\|_\infty = M.$$

On the interval where $u_1 > \alpha M$ the solution is rescaled further, yielding u_2, and so forth.

The $(k+1)$-st rescaled solution u_{k+1} is introduced when τ_k, the "clock" for u_k, reaches a value τ_k^* such that

$$\|u_k(\cdot, \tau_k^*)\|_\infty = M. \tag{2.13}$$

The interval in y_k-space to be rescaled, (y_k^-, y_k^+), consists precisely of the grid points where $u_k(\cdot, \tau_k^*) \geqq \alpha M$:

$$\begin{aligned} u_k(y_k^- - \Delta y_k, \tau_k^*) &< \alpha M \leqq u_k(y_k^-, \tau_k^*), \\ u_k(y_k^+, \tau_k^*) &\geqq \alpha M > u_k(y_k^+ + \Delta y_k, \tau_k^*). \end{aligned} \tag{2.14}$$

The next rescaled solution u_{k+1} is related to u_k by

$$u_{k+1}(y_{k+1}, \tau_{k+1}) = \lambda^{2/(p-1)} u_k(\lambda y_{k+1}, \tau_k^* + \lambda^2 \tau_{k+1}); \tag{2.15}$$

its "rescaled space" and "rescaled time" variables y_{k+1} and τ_{k+1} range over

$$\lambda^{-1} y_k^- \leqq y_{k+1} \leqq \lambda^{-1} y_k^+, \qquad \tau_{k+1} \geqq 0. \tag{2.16}$$

Its initial data $u_{k+1}(y_{k+1}, 0)$ are determined by rescaling $u_k(\cdot, \tau_k^*)$, using linear interpolation to define it on a refined spatial grid of mesh width $\Delta y_{k+1} = \Delta x$. Its boundary data $u_{k+1}(\lambda^{-1} y_k^\pm, N\Delta\tau_{k+1})$ are determined from u_k using the coarse mesh approximation, and it is stepped forward in time by the forward Euler difference scheme with $\Delta\tau_{k+1} = \Delta t$. Previously rescaled solutions are stepped forward independently: if for example $\lambda = \frac{1}{4}$, then u_k is stepped forward once every 16 time steps of u_{k+1}, u_{k-1} once every 256 time steps of u_{k+1}, etc. Whenever a fine grid solution is computed at a point in space-time where a coarser mesh solution is also defined, the value of the coarse mesh solution is updated to agree with the fine grid calculation. When a time step is reached such that $\|u_{k+1}(\cdot, N\Delta\tau)\|_\infty > M$, then it is time for another rescaling. A smaller time step is used to find τ_{k+1}^* such that $\|u_{k+1}(\cdot, \tau_{k+1}^*)\|_\infty = M$, and the entire procedure is repeated.

This algorithm cannot be continued indefinitely without losing accuracy. We use the symmetry of the computed solution as an indicator of the accuracy of the calculation. With symmetric initial data and perfect arithmetic, u_k would remain symmetric for every k. However, the roundoff error is not symmetric. In a typical calculation using $\lambda = \frac{1}{2}$, the amplitude of the asymmetry approximately doubles from one rescaling to the next. On a Cray XMP using double precision arithmetic, machine epsilon is about 10^{-26}, and by the 87-th iteration only two or three digits of symmetry remain. Generally we stop the calculation after 80 iterations; with $p = 5$ and $\lambda = \frac{1}{2}$, the corresponding amplitude of u is on the order of $(\lambda^{-2/(p-1)})^{80} \approx 10^{12}$. The use of multiple grids, rescaling and refining only where the solution is large, is crucial to the success of this calculation: to achieve similar results without mesh refinement on a single, uniform grid would require 10^{26} mesh points! Similar accuracy could be achieved using a single nonuniform grid (c.f. [24], [25]) but our method has the advantage of choosing the proper distribution of grid points automatically.

Certain qualitative features of the solution are strikingly clear from even a casual examination of the output of our algorithm:

(2.17a) The "rescaling times" τ_k^* are eventually almost independent of k (Figure 2).

(2.17b) If $u_k(\cdot, \tau_k^*)$ is graphed over a fixed interval, say $-1 < z < 1$, then the graph is eventually independent of k (Figures 3, 4).

(2.17c) The width of the interval rescaled at the k-th iteration behaves as the square root of a linear function (Figure 5).

All these assertions are explained in Section 4. It turns out that (2.17a) is a consequence of the (proved) result (1.3), while (2.17b,c) are related to the conjectured asymptotics (1.4).

3. Review of the Theory

Before interpreting the algorithm, we review some of the results and conjectures concerning the blow-up of u. Our discussion is restricted for simplicity to the case at hand: positive, symmetric, radially decreasing solutions of (1.1) on an interval with a Dirichlet boundary condition. It should be noted, however, that parts of the theory have been carried out in much greater generality, including space dimensions $n > 1$ and non-radial solutions.

Let T be the blow-up time of u, in other words,

$$\|u(\cdot, t)\|_\infty = u(0, t) \to \infty \quad \text{as} \quad t \uparrow T.$$

It is convenient to introduce "similarity variables", a change of both dependent and independent variables defined by

$$\begin{aligned} w(\xi, s) &= (T - t)^{1/(p-1)} u(x, t), \\ \xi &= x/\sqrt{T - t}, \\ s &= -\log(T - t). \end{aligned} \tag{3.1}$$

One computes that u solves (1.1) if and only if

$$w_s - w_{\xi\xi} + \frac{1}{2}\xi w_\xi + \frac{1}{p-1}w - w^p = 0. \tag{3.2}$$

Since $s \to \infty$ as $t \uparrow T$, the change of variables (3.2) converts any question about the blow-up of u into one about the large time asymptotics of w.

Upper and lower bounds are known for the blow-up rate of u (see [11]); they imply that

$$0 < C \leqq \|w(\cdot, s)\|_\infty = w(0, s) \leqq C' < \infty \tag{3.3}$$

for some positive C, C', independent of s. Rewriting the equation (3.2) as

$$w_s - \frac{1}{\rho}(\rho w_\xi)_\xi + \frac{1}{p-1}w - w^p = 0$$

with $\rho(\xi) = \exp\{-\frac{1}{4}\xi^2\}$, it is easy to see that

$$E[w] = \int\left[\frac{1}{2}w_\xi^2 + \frac{1}{2(p-1)}w^2 - \frac{1}{p+1}|w|^{p+1}\right]\rho(\xi)\,d\xi$$

decreases as s increases, and indeed that

$$\frac{d}{ds}E[w] \leqq -\int w_s^2\rho\,d\xi.$$

It is thus natural to expect that, as $s \to \infty$, $w(\xi, s)$ should tend to a stationary point $w_\infty(\xi)$ of the functional E. It turns out that the only stationary points of E are the "trivial" ones $w_\infty \equiv 0$ and $w_\infty \equiv \pm(p-1)^{-1/(p-1)}$. Since the nonpositive stationary points are ruled out by (3.3), we are led (heuristically) to the conclusion that, as $s \to \infty$, $w(\xi, s)$ should tend to the constant function $w_\infty(\xi) \equiv (p-1)^{-1/(p-1)}$. These ideas can be made rigorous, and they lead to

THEOREM 3.1 [14], [16]. *As $s \to \infty$, $w(\xi, s) \to (p-1)^{-1/(p-1)}$, uniformly on the set $|\xi| < C$ for any $C > 0$.*

Transformed into the original variables via (3.1) this is equivalent to (1.3).

Now consider the profile of w as a function of ξ for fixed $s \gg 1$. Evidently it is nearly flat, $w \approx (p-1)^{-1/(p-1)}$, on an interval about the origin which grows with s; but it decays to 0 at the endpoints $\xi = \pm e^{s/2}$, corresponding to $x = \pm 1$. The form of this profile can be guessed by supposing that $w(\xi, s) \sim f(\xi/g(s))$ for some functions $f(\eta)$ and $g(s)$; cf. [14], [20]. To obtain the expected qualitative behavior we suppose that

$$g(s) \uparrow \infty \quad \text{as} \quad s \to \infty, \tag{3.4a}$$

and

$$f(0) = (p-1)^{-1/(p-1)}, \qquad f(\eta) \to 0 \quad \text{as} \quad |\eta| \to \infty; \tag{3.4b}$$

moreover, for reasons that will emerge shortly, we also want to assume that

$$g'(s)/g(s) \to 0 \quad \text{as} \quad s \to \infty, \tag{3.4c}$$

i.e., that g has subexponential growth. Substitution of the ansatz into the equation yields

$$-\frac{g'(s)}{g(s)}\eta f'(\eta) - g^{-2}(s) f''(\eta) + \frac{1}{2}\eta f'(\eta) + \frac{1}{p-1} f(\eta) - f^p(\eta) \sim 0. \tag{3.5}$$

As $s \to \infty$, the first two terms tend to 0 by virtue of (3.4a, c), leading to this first-order equation for f:

$$\frac{1}{2}\eta f'(\eta) + \frac{1}{p-1} f(\eta) - f^p(\eta) = 0. \tag{3.6}$$

The general solution is

$$f(\eta) = \left((p-1) + c\eta^2\right)^{-1/(p-1)}, \tag{3.7}$$

in which $c > 0$ is an arbitrary constant of integration. Notice that f satisfies (3.4b) regardless of the choice of c. Absorbing the constant of integration into the (unknown) g leads to

CONJECTURE 3.2. *$w(\xi, s) \sim ((p-1) + \xi^2/g^2(s))^{-1/(p-1)}$ for some $g(s)$ such that $g \to \infty$ and $g'/g \to 0$ as $s \to \infty$.*

This is consistent with Theorem 3.1 since $\xi^2/g(s)^2 \to 0$ as $s \to \infty$ with $|\xi| < C$. As will be explained in Section 4, it is borne out by our calculations, and indeed is responsible for the observed stability of the profile of u_k, (2.17b). In terms of the original variables, this conjecture says that

$$u(x,t) \sim (T-t)^{\frac{-1}{p-1}} \left((p-1) + \frac{x^2}{(T-t)g^2(|\log(T-t)|)}\right)^{\frac{-1}{p-1}}. \tag{3.8}$$

So far we have guessed the profile f, but not the spreading rate g. A formal procedure for determining g is worked out in [13], [14], following a method introduced in [20]. The idea is to look for a formal expansion in powers of s^{-1},

$$w(\xi, s) \sim f_0(\xi/g(s)) + \frac{1}{s} f_1(\xi/g(s)) + \cdots, \tag{3.9}$$

and to suppose that the first two terms of (3.9) interact by setting

$$g(s) = c_0 s^{1/2}. \tag{3.10}$$

(The expansion (3.9) would appear to be consistent with other choices, for example $g(s) = c_0 s$, but for such g it becomes impossible to satisfy the consistency condition (3.16) below.) The value of the constant c_0 is determined by a consistency condition for the existence of f_1, as we now explain. Substitution of the ansatz (3.9) into the equation (3.2) gives a sequence of equations of orders s^0, s^{-1}, s^{-2}, etc. The first says that f_0 satisfies (3.6); we may choose the constant of integration to be 1 in (3.7), since c_0 is as yet undetermined in (3.10):

$$f_0(\eta) = ((p-1) + \eta^2)^{-1/(p-1)}. \tag{3.11}$$

The order s^{-1} equation says that

$$-\frac{1}{2}\eta f_0' - c_0^{-2} f_0'' + \frac{1}{2}\eta f_1' + \frac{1}{p-1} f_1 - p f_0^{p-1} f_1 = 0. \tag{3.12}$$

Using (3.11), this takes the form

$$f_1' + \alpha(\eta) f_1 = \frac{1}{\eta}\beta(\eta) \tag{3.13}$$

with

$$\alpha(\eta) = \frac{2}{\eta}\left[\frac{1}{p-1} - \frac{p}{(p-1)+\eta^2}\right], \qquad \beta(\eta) = \eta f_0' + 2c_0^{-2} f_0''. \tag{3.14}$$

We can write (3.13) as

$$e^{-A}(e^{A} f_1)' = \frac{1}{\eta}\beta(\eta),$$

where A is any indefinite integral of α. One computes that

$$e^{A} = C f_0^{-p}\eta^{-2};$$

hence the general solution of (3.12) is

$$f_1(\eta) = f_0^p \eta^2\left[c_1 + \int_1^\eta t^{-3} f_0^{-p}(t)\beta(t)\,dt\right], \tag{3.15}$$

with $c_1 \in \mathbb{R}$ a new constant of integration. The rule proposed in [20] for choosing c_0 is to require that

(3.16) $\qquad f_1$ should be analytic at $\eta = 0$.

In other words, the coefficient of t^2 in the Taylor expansion

$$f_0^{-p}(t)\beta(t) = a_0 + a_1 t + a_2 t^2 + \cdots \tag{3.17}$$

should vanish, so that the corresponding term $f_0^p \eta^2 \log(\eta)$ is absent from (3.15). The logic behind this requirement is that such a logarithmic term would be differentiated in the process of finding $f_2, f_3, \cdots$, and would eventually lead to a term that is infinite at $\eta = 0$. Calculation gives that

$$a_2 = 0 \quad \text{in} \quad (3.17) \leftrightarrow c_0^2 = \frac{4p}{(p-1)^2}. \tag{3.18}$$

The first term in the expansion (3.9) is now entirely determined. Since our numerical results are insufficient to resolve the next term, there is no need to evaluate the integral (3.15) for f_1. However, we shall make use of its value at $\eta = 0$. From (3.15) and (3.17),

$$f_1(0) = -\tfrac{1}{2} f_0^p(0) a_0 = -\tfrac{1}{2}\beta(0),$$

where β is given by (3.14). Calculation gives

$$-\frac{1}{2}\beta(0) = -c_0^{-2} f_0''(0) = \frac{1}{2p}(p-1)^{-1/(p-1)}.$$

We are thus led to this refinement of Conjecture 3.2:

CONJECTURE 3.3 [13], [14]. *Asymptotically as $s \to \infty$,*

$$w(\xi, s) = (p-1)^{-1/(p-1)}\left[1 + \frac{p-1}{4p}\xi^2 s^{-1}\right]^{-1/(p-1)} + O(s^{-1}). \tag{3.19a}$$

Moreover, at $\xi = 0$ the order s^{-1} correction to (3.19a) is given by

$$w(0, s) = (p-1)^{-1/(p-1)}\left[1 + \frac{1}{2p}s^{-1}\right] + O(s^{-2}). \tag{3.19b}$$

Rewritten in terms of the original variables $u(x, t)$, the first assertion is precisely (1.4).

The preceding calculation is purely formal: we know of no proof that the expansion (3.9) can be continued to all orders, or that it correctly represents the behavior of w. However, there is some theoretical support for (3.10): it is known (see [10]) that $w(\xi, s) \to 0$ as $s \to \infty$ with $|\xi|/(s^{1/2}) \to \infty$. This implies that if Conjecture 3.2 is valid for some function $g(s)$, then $g \leq cs^{1/2}$. (A similar result is proved for a slightly different boundary value problem in [14].) As we shall explain presently, the spreading rate $g(s)$ is linked to the width of the interval rescaled at each stage of our algorithm; moreover, the linear growth of $(y_k')^2$ asserted in (2.17c) reflects the conjectured behavior $g = c_0 s^{1/2}$.

4. Numerical Results and Interpretation

In this section we use our numerical results to test the conjectures described above. The interpretation of the results is complicated by the presence of two sources of error: the discretization error in using the forward Euler scheme on a finite grid, and the asymptotic error, which arises since the conjectures refer only to the behavior of $w(\xi, s)$ as $s \to \infty$.

All the runs reported here use $\phi(x) = 1 + \cos(\pi x)$ as the initial data, $p = 5$ for the nonlinearity, and $\lambda = \frac{1}{2}$, $M = 2\sqrt{2}$, $\alpha = 1.8/2\sqrt{2}$ for the parameters of the algorithm. These values are typical but arbitrary: other choices of initial data and algorithm parameters lead to identical conclusions about the asymptotic character of the blow-up. The values of Δx and Δt are always chosen so that $\Delta t/(\Delta x)^2 = .25$, and each run is continued for eighty rescaling iterations. Since the algorithm is an unusual one, combining rescaling and grid refinement, we do a convergence study for $\Delta x = .02$, .01, and .005 corresponding, respectively, to 100, 200, and 400 points in the initial grid for $u(x, 0)$.

In order to relate our calculations to the conjectures it is necessary to connect the computed "rescaled solutions" $u_k(y_k, \tau_k)$ with the "real" solution $u(x, t)$ and the "solution in similarity variables" $w(\xi, s)$. This may at first glance appear impossible, since u_k is related to u_{k-1} (and hence ultimately to u) by the scaling (2.15), which takes place at the implicitly defined time τ_k^*, while w is related to u by the change of variables (3.1), which involves the unknown blow-up time T. In fact, however, it is possible: the missing link is Theorem 3.1, which relates $(T - t)$ to the magnitude of u, asymptotically as $t \to T$.

The first task is to express $u_k(y_k, \tau_k)$ in terms of $u(x, t)$, the solution of (1.1). If t_k is the "real" time at which the rescaling from u_k to u_{k+1} takes place, then (2.15) gives

$$t_k = \tau_0^* + \lambda^2 \tau_1^* + \cdots + \lambda^{2k} \tau_k^*, \tag{4.1}$$

where τ_i^* is the scaled time at which u_i is rescaled to create u_{i+1}. Iteration of (2.15) also gives a formula for the computed rescaled solution u_k just before the next rescaling:

$$u_k(y_k, \tau_k^*) = \lambda^{2k/(p-1)} u(\lambda^k y_k, t_k), \tag{4.2}$$

where y_k is the spatial variable of u_k. In particular, at time t_k the amplitude of u has increased by a factor of $\lambda^{-2k/(p-1)}$,

$$\|u(\cdot, t_k)\|_\infty = u(0, t_k) = \lambda^{-2k/(p-1)} M, \tag{4.3}$$

and so the blow-up time is $T = \lim_{k \to \infty} t_k$.

Our qualitative observation (2.17a) is concerned with the number of time steps taken on the grid for u_k before the creation of u_{k+1}. Let us call this number $N_k(100)$ when the initial grid has 100 points, and so forth. Recall that τ_k represents the "scaled time" for u_k (see (2.15)), and that u_{k+1} is created at $\tau_k = \tau_k^*$. Since we use the same time step $\Delta\tau_k = \Delta t$ for every k, N_k would be $(\Delta t)^{-1}\tau_k^*$ in the absence of discretization error. To understand the behavior as $k \to \infty$, we write (1.3) in the form

$$(T - t_k)u(0, t_k)^{p-1} = \frac{1}{p-1} + o(1), \tag{4.4}$$

where $o(1)$ represents a term that tends to 0 as $k \to \infty$. When combined with (4.3) this gives an asymptotic formula for $T - t_k$ in terms of k:

$$(T - t_k)\lambda^{-2k} = M^{1-p} \cdot \frac{1}{p-1} + o(1). \tag{4.5}$$

The behavior of τ_k^* as $k \to \infty$ is determined by (4.1) and (4.5):

$$\begin{aligned}\tau_k^* &= \lambda^{-2k}(t_k - t_{k-1}) \\ &= \lambda^{-2k}((T - t_{k-1}) - (T - t_k)) \\ &= M^{1-p} \cdot \frac{1}{p-1}(\lambda^{-2} - 1) + o(1),\end{aligned}$$

so that

$$\lim_{k\to\infty} \tau_k^* = M^{1-p} \cdot \frac{1}{p-1}(\lambda^{-2} - 1). \tag{4.6}$$

Thus the number of time steps N_k should become asymptotically independent of k. This is precisely what happens: Figure 2 shows $N_k\,\Delta t$ as a function of k, for computations using 100, 200 and 400 grid points initially, and Table 1 gives the values of N_k at selected values of k.

The preceding argument was based on the rigorous result (1.3). More detailed asymptotics for τ_k^* can be obtained from the conjectured behavior (3.19b), which gives a $1/s$ correction to the amplitude of $w(0, s)$ as $s \to \infty$. To this end, let $s_k = -\log(T - t_k)$, and note from (4.5) that

$$s_k = 2|\log\lambda|k + [\log(p-1) + (p-1)\log M] + o(1). \tag{4.7}$$

From (3.19b) we have

$$w(0, s_k)^{p-1} = \frac{1}{p-1}\left(1 + \frac{p-1}{2p}s_k^{-1}\right) + O(s_k^{-2}).$$

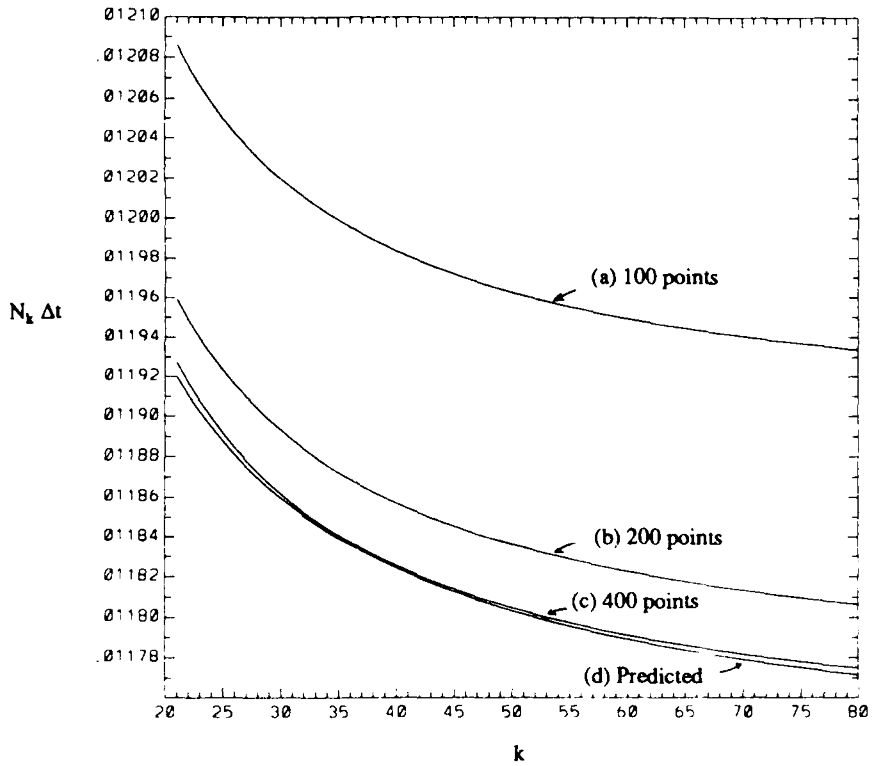

Figure 2. The computed time $N_k\,\Delta t$ until the amplitude of u_k reaches threshold M, plotted against k, when the initial grid has (a) 100 points, (b) 200 points, (c) 400 points. Curve (d) is the predicted value $N_k^{\text{asymp}}\,\Delta t$ from (4.9).

Table I. Number of steps on each grid until the amplitude reaches threshold.

k	$N_k(100)$	$N_k(200)$	$N_k(400)$
20	120.98	478.82	1910.21
30	120.20	475.73	1897.88
40	119.84	474.28	1892.09
50	119.63	473.45	1888.76
60	119.50	472.91	1886.60
70	119.40	472.53	1885.09
80	119.34	472.25	1883.98

Using (4.7) and the definition of w, (3.1), we obtain

$$(T - t_k)u(0, t_k)^{p-1} = \frac{1}{p-1}\left(1 + \frac{p-1}{4p|\log\lambda|}\frac{1}{k}\right) + O(k^{-2}),$$

strengthening (4.4). This leads to

$$(T - t_k)\lambda^{-2k} = M^{1-p}\frac{1}{p-1}\left(1 + \frac{p-1}{4p|\log\lambda|}\frac{1}{k}\right) + O(k^{-2}),$$

in place of (4.5), whence

$$\tau_k^* = \lambda^{-2k}((T - t_{k-1}) - (T - t_k))$$

$$= M^{1-p}\cdot\frac{1}{p-1}(\lambda^{-2} - 1)\left(1 + \frac{p-1}{4p|\log\lambda|}\frac{1}{k}\right) + O(k^{-2}). \tag{4.8}$$

We are thus led, by neglecting the error term in (4.8), to an asymptotic formula for N_k:

$$N_k^{\text{asymp}} = (\Delta t)^{-1}\cdot M^{1-p}\cdot\frac{1}{p-1}(\lambda^{-2} - 1)\left(1 + \frac{p-1}{4p|\log\lambda|}\cdot\frac{1}{k}\right). \tag{4.9}$$

The graph of $N_k^{\text{asymp}}\cdot\Delta t$ is the lowest line in Figure 2; it deviates from the values computed using the finest mesh by only about .05%. As another test of (4.9), we note from Table 1 that when 400 initial grid points are used, the number of time steps per iteration changes by only 2.62 between $k = 60$ and $k = 80$. For our choices of λ, p, and M, and with $\Delta t = .25(\Delta x)^2 = 6.25\cdot 10^{-6}$, (4.9) gives

$$N_{60}^{\text{asymp}} - N_{80}^{\text{asymp}} = 2.25,$$

in approximate agreement with the computation.

The observed values of N_k can also be used to test the convergence of the calculations as $\Delta x \to 0$. Focusing on $k = 80$, we see that the error $E = |N_{80} - N_{80}^{\text{asymp}}|\cdot\Delta t$ is

$$E(400) = 6.73\cdot\Delta t_{400},$$

$$E(200) = 2.94\cdot\Delta t_{200} = 11.76\cdot\Delta t_{400},$$

$$E(100) = 2.01\cdot\Delta t_{100} = 32.16\cdot\Delta t_{400},$$

reflecting the first-order convergence rate in time of the difference scheme.

Our second qualitative observation is concerned with the computed rescaled solution just prior to the next rescaling, $u_k(y_k, \tau_k^*)$. It is defined for $-\lambda^{-1}y_{k-1}^- < y_k < \lambda^{-1}y_{k-1}^+$, an interval that grows with k. To compare the profiles for different values of k, it is therefore convenient to rescale each $u_k(y_k, \tau_k^*)$ so as to make it be defined on a fixed interval $-1 < z < 1$. (Beware: this last rescaling affects space alone, not the values of u_k; it has nothing to do with the rescalings that are done in the course of the algorithm.) Since by symmetry $y_{k-1}^- \approx y_{k-1}^+$, we are led to consider the "rescaled profile"

$$z \to u_k\left(z\lambda^{-1}y_{k-1}^+, \tau_k^*\right), \qquad -1 < z < 1. \tag{4.10}$$

Our observation (2.17b) asserts that this function is asymptotically independent of k.

In fact, as we shall now explain, the form of this rescaled profile can be predicted from our cruder Conjecture 3.2 alone. Indeed, suppose that

$$w(\xi, s) = f(\xi/g(s)) + o(1) \tag{4.11}$$

with f and g as in (3.4a–c). To relate $u_k(y_k, \tau_k^*)$ and w, we combine (4.2) and (3.1):

$$u_k(y_k, \tau_k^*) = \lambda^{2k/(p-1)}(T - t_k)^{-1/(p-1)}w\left(\lambda^k y_k(T - t_k)^{-1/2}, s_k\right), \tag{4.12}$$

with $s_k = -\log(T - t_k)$, as above. Since w is a uniformly continuous function of its arguments (see for example [16]), (4.5) and (4.12) yield

$$u_k(y_k, \tau_k^*) = (p-1)^{1/(p-1)}Mw\left(\sqrt{p-1}\,M^{(p-1)/2}y_k, s_k\right) + o(1). \tag{4.13}$$

Substitution of (4.11) into (4.13) yields the corresponding prediction for (4.10).

$$\begin{aligned} &u_k\left(z\lambda^{-1}y_{k-1}^+, \tau_k^*\right) \\ &\quad = (p-1)^{1/(p-1)}Mf\left(\sqrt{p-1}\,M^{(p-1)/2}z\lambda^{-1}y_{k-1}^+/g(s_k)\right) + o(1). \end{aligned}$$

The asymptotic behavior is evidently governed by that of the ratio $y_{k-1}^+/g(s_k)$. This, too can be evaluated by substituting the ansatz (4.11) into the known relation between u_k and w, (4.13). In fact, ignoring errors of computation for the moment, we set $\Delta x = 0$ in the definition of y_{k-1}^+, (2.14), to get

$$u_{k-1}\left(y_{k-1}^+, \tau_{k-1}^*\right) = u_{k-1}\left(y_{k-1}^-, \tau_{k-1}^*\right) = \alpha M. \tag{4.14}$$

Therefore, from (4.13) and (4.14), we have

$$\alpha M = (p-1)^{1/(p-1)}Mf\left(\sqrt{p-1}\,M^{(p-1)/2}y_{k-1}^+/g(s_{k-1})\right) + o(1),$$

so that $y_{k-1}^+/g(s_{k-1})$ tends as $k \to \infty$ to the (positive) root ζ of

$$\alpha = (p-1)^{1/(p-1)}f\left(\sqrt{p-1}\,M^{(p-1)/2}\zeta\right). \tag{4.15}$$

The observed ratio $y_{k-1}^{+}/g(s_k)$ has the same asymptotic value, since by Taylor's theorem

$$\frac{g(s_k)}{g(s_{k-1})} - 1 \leqq \max_{s_{k-1} \leqq \sigma \leqq s_k} \frac{g'(\sigma)}{g(s_{k-1})}(s_k - s_{k-1});$$

using this, the known asymptotics of s_k, (4.7), and the growth hypothesis on g, (3.4c), one easily shows that

$$\lim_{k \to \infty} \frac{g(s_k)}{g(s_{k-1})} = 1.$$

We conclude that if w has the proposed form (4.11), then the rescaled profile of u_k, (4.10), is asymptotically

$$z \to (p-1)^{1/(p-1)} M f\left(\sqrt{p-1}\, M^{(p-1)/2} \lambda^{-1} \zeta z\right). \tag{4.16}$$

Notice that the predicted profile (4.16) depends only on f, not on the "spreading rate" $g(s)$: the effect of g has been washed out by the final rescaling of u_k.

Conjecture 3.2 asserts not only that w has the asymptotic behavior $f(\xi/g(s))$ but also the form of f:

$$f(\eta) = \left((p-1) + \eta^2\right)^{-1/(p-1)}.$$

The root ζ of (4.15) is easily computed to be

$$\zeta = M^{(1-p)/2}(\alpha^{1-p} - 1)^{1/2}, \tag{4.17}$$

and substitution into (4.16) yields

$$u_k(z\lambda^{-1} y_{k-1}^{+}, \tau_k^{*}) \sim M\left[1 + (\alpha^{1-p} - 1)\lambda^{-2} z^2\right]^{-1/(p-1)}. \tag{4.18}$$

The right side of (4.18) is virtually indistinguishable from the output of our algorithm after sufficiently many iterations, see Figures 3 and 4. A quantitative study of the convergence rate is difficult, since in the computation the set where $u > \alpha M$ is enlarged to include an additional grid point on either side when rescaling and refinement is done. However, the qualitative behavior can be seen by evaluating (4.18) at $z = \frac{1}{2}$, and comparing it with the rescaled computed solution at $z = \frac{1}{2}$ after $k = 80$ iterations, using 100, 200 and 400 points in the initial spatial grid:

left side of (4.18) using 100 grid points = 1.8081,

left side of (4.18) using 200 grid points = 1.8064,

left side of (4.18) using 400 grid points = 1.8047,

right side of (4.18) = 1.8.

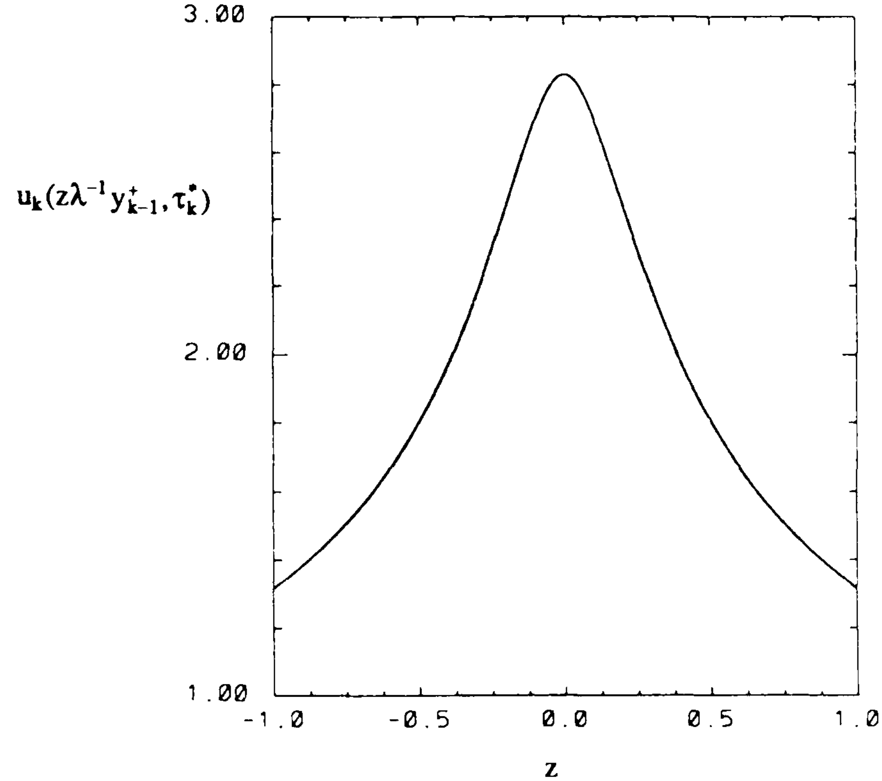

Figure 3. The computed profile of u_k rescaled as in (4.10) at $k = 80$, and the predicted profile (4.18). They coincide to within plotting resolution.

Recall also that the right-hand side of (4.18) does not include a $1/k$ correction term, but is the asymptotic limit as $k \to \infty$.

Our third qualitative observation is that $(y_k^+)^2$ grows linearly with k. This is linked to the "spreading rate" g in (4.11), since the discussion leading to (4.16) shows that

$$y_k^+ = g(s_k)(\zeta + o(1)), \tag{4.19}$$

where ζ is the root of (4.15). Conjecture 3.3 asserts that

$$g(s_k) = c_0 s_k^{1/2}, \qquad c_0^2 = \frac{4p}{(p-1)^2};$$

combined with the asymptotics of s_k, (4.7), and the value of ζ, (4.17), this yields

$$(y_k^+)^2 = k \cdot \frac{8p}{(p-1)^2} |\log \lambda| M^{1-p}(\alpha^{1-p} - 1) + o(k). \tag{4.20}$$

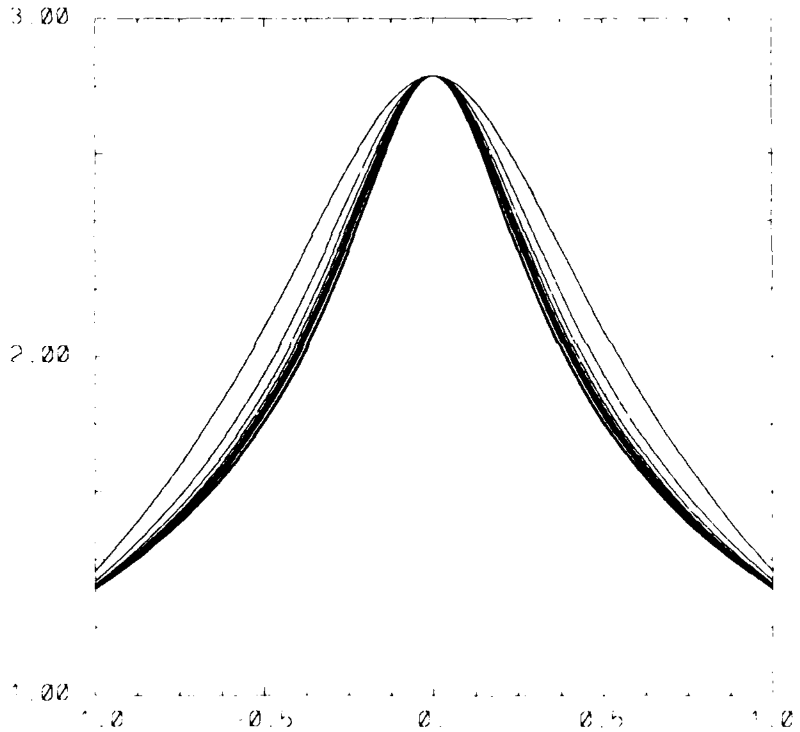

Figure 4. The computed profiles of u_k for selected values of k, each rescaled as in (4.10). As k increases they converge to the profile shown in Figure 3.

As in the last paragraph, we expect the right side of (4.20) to be an expansion in powers of k. In particular, if (3.19a) is used in place of (4.11) in the derivation of (4.19), then $o(1)$ becomes $O(1/k)$ and (4.20) becomes

$$(4.21) \qquad (y_k^+)^2 = k \cdot \frac{8p}{(p-1)^2} |\log \lambda| M^{1-p}(\alpha^{1-p} - 1) + O(1).$$

Thus, Conjecture 3.3 predicts not only that $(y_k^+)^2$ is asymptotically linear, but also the value of the slope.

For making a quantitative comparison between our numerical results and the conjectured behavior, there is a slight advantage to replacing y_k^+ in the above arguments by the point y_k^θ defined by

$$(4.22) \qquad u_k(y_k^\theta, \tau_k^*) = \theta M,$$

with θ chosen so that $\alpha < \theta < 1$. The reason is that the numerically computed y_k^+ does not satisfy (4.14) exactly, since it is required to be a grid point, see (2.14).

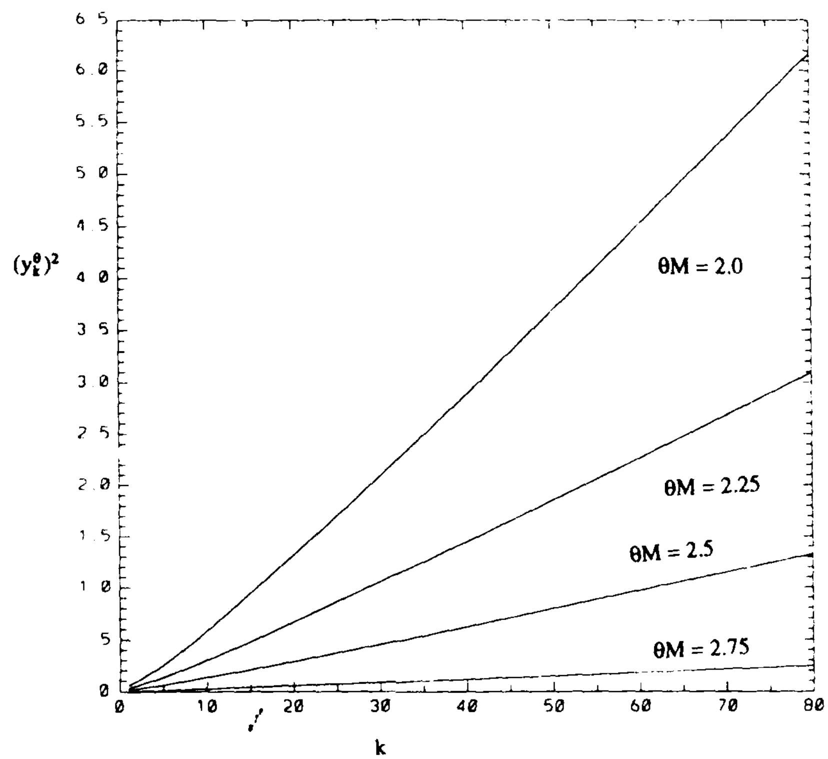

Figure 5. The graph of $(y_k^\theta)^2$ against k, for various values of θ, based on data obtained using 400 points in the initial grid. The width of the interval rescaled at the kth iteration is $2y_k^\alpha$, with α as in (2.2).

However, y_k^θ need not be a grid point, so it can be chosen to solve (4.22) exactly (within the accuracy of the calculation) by using linear interpolation in space. Replacing α by θ in the arguments that led to (4.21) we see that $(y_k^\theta)^2$ is expected to grow as

$$(4.23)\quad (y_k^\theta)^2 = \gamma \cdot k + O(1), \qquad \gamma = \frac{8p}{(p-1)^2}|\log \lambda| M^{1-p}(\theta^{1-p} - 1).$$

Thus the points $(k, (y_k^\theta)^2)$, with θ held fixed, should approach a line of slope γ. Our values for p, M, and λ give $\gamma = .027(\theta^{-4} - 1)$. Figure 5 shows $(y_k^\theta)^2$ as a function of k for several values of θ, using 400 points in the initial grid. For a quantitative comparison, we present in Table 2 the slope of the line which best fits the points $(k, (y_k^\theta)^2)$ in the least squares sense for $60 < k < 80$, and for several different values of θ. The results agree with the prediction (4.23) to within 3%.

Table II. Slope of line through the points $(k, (y_k^\theta)^2)$, where $u_k(y_k^\theta, \tau_k^*) = \theta M$.

θM	computed slope	predicted slope
2.0	.08327	.08123
2.25	.04156	.04054
2.5	.01772	.01729
2.75	.00330	.00322

5. Conclusions

We have demonstrated the convergence of the rescaling algorithm, and used it to calculate the solution of $u_t - u_{xx} = u^5$ until its magnitude reaches about 10^{12}. The computed singularity is consistent with the conjectured form (1.4), derived by means of a formal expansion.

This method appears to be suitable for computing singularities that arise in the solutions of other equations with a similar scale invariance. Although we obtain satisfactory results using the forward Euler scheme, which is just first-order accurate in time, it may be better for some applications to use a more accurate discretization of the partial differential equation. A natural candidate for further investigation is the nonlinear Schrödinger equation $iu_t - \Delta u - |u|^{p-1}u = 0$ on a ball in $\mathbb{R}^n$ with radial initial data and a Dirichlet boundary condition, in the critical $p = (n + 4)/n$ or supercritical $p > (n + 4)/n$ cases. Though extensive calculations have already been done (see [24], [25], [27]), we think that our algorithm may achieve a greater resolution of the local behavior of the singularity than those done to date.

Acknowledgments. We would like to thank Jonathan Goodman and Luis Reyna for suggesting that this problem could be approached using adaptive mesh refinement.

This work was partially supported by grants from AFOSR, DOE, DARPA, NSF, ONR, and the Sloan Foundation.

Bibliography

[1] Baras, P., and Cohen, L., *Complete blow-up after T_{max} for the solution of a semilinear heat equation*, to appear.

[2] Bebernes, J., and Eberly, D., *A description of self-similar blow-up for dimension $n \geq 3$*, Ann. Inst. H. Poincaré-Analyse Nonlineaire, 5, 1988, pp. 1–22.

[3] Berger, M., *Stability of interfaces with mesh refinement*, Math. Comp. 45, 1985, pp. 301–318.

[4] Berger, M., and Oliger, J., *Adaptive mesh refinement for hyperbolic partial differential equations*, J. Comp. Phys. 53, 1984, pp. 484–512.

[5] Chen, Y.-G. *On blow-up solutions of semilinear parabolic equations: analytical and numerical studies*, Thesis, Tokyo University, 1987.

[6] Chen, Y.-G., *Asymptotic behavior of blowing-up solutions for finite difference analogue of $u_t = u_{xx} + u^{1+\alpha}$*, J. Fac. Sci. Univ. Tokyo Sect. IA (Math) 33, 1986, pp. 541–574.

[7] Chorin, A., *Estimates of intermittency, spectra, and blow-up in developed turbulence*, Comm. Pure Appl. Math. 34, 1981, pp. 853–866.

[8] Ciment, M., *Stable difference schemes with uneven mesh spacings*, Math. Comp. 25, 1971, pp. 219–227.

[9] Dold, J. W., *Analysis of the early stage of thermal runaway*, Q. J. Mech. Appl. Math. 38, 1985, pp. 361–387.

[10] Friedman, A., *Blowup of solutions of nonlinear parabolic equations*, in Proc. of Microprogram on Nonlinear Diffusion Equations and their Equilibrium States, MSRI, Berkeley, 1986, to appear.

[11] Friedman, A., and McLeod, B., *Blowup of positive solutions of semilinear heat equations*, Indiana Univ. Math. J. 34, 1985, pp. 425–447.

[12] Fujita, H., and Chen, Y.-G., *On the set of blowup points and asymptotic behavior of blowup solutions to a semilinear parabolic equation*, Analyse Math. et Appl., to appear.

[13] Galaktionov, V. A., and Posashkov, S. A., *The equation $u_t = u_{xx} + u^\beta$. Localization and asymptotic behavior of unbounded solutions*, Preprint no. 97, Keldysh Institute of Applied Math., Moscow, 1985. (In Russian.)

[14] Galaktionov, V. A., and S. A. Posashkov, S. A., *Application of a new comparison theorem to the study of unbounded solutions of nonlinear parabolic equations*, Differ. Uravnen. 22, 1986, pp. 1165–1173. (In Russian.)

[15] Giga, Y., *Self-similar solutions for semilinear parabolic equations*, in *Nonlinear Systems of Partial Differential Equations in Applied Mathematics*, B. Nicolaenko et al. eds., AMS Lecture Notes in Appl. Math. 23, 1986, Part 2, pp. 247–252.

[16] Giga, Y., and Kohn, R. V., *Asymptotically self-similar blow-up of semilinear heat equations*, Comm. Pure Appl. Math. 38, 1985, pp. 297–319.

[17] Giga, Y., and Kohn, R. V., *Characterizing blow-up using similarity variables*, Indiana Univ. Math. J. 36, 1987, pp. 1–40.

[18] Giga, Y., and Kohn, R. V., *Removability of blow-up points for semilinear heat equations*, to appear in proc. EQUADIFF, G. Papanicolaou, ed., Marcel Dekker, 1987.

[19] Giga, Y., and Kohn, R. V., *Nondegeneracy of blow-up for semilinear heat equations*, preprint.

[20] Hocking, L. M., Stewartson, K., and Stuart, J. T., *A nonlinear instability burst in plane parallel flow*, J. Fluid Mech. 51, 1972, pp. 705–735.

[21] Kapila, A. K., *Reactive-diffusive system with Arrhenius kinetics: dynamics of ignition*, SIAM J Appl. Math. 39, 1980, pp. 21–36.

[22] Kassoy, D., and Poland, J., *The thermal explosion confined by a constant temperature boundary: I. The induction period solution*, SIAM J. Appl. Math. 39, 1980, pp. 412–430.

[23] Lacey, A. A., *The form of blowup for nonlinear parabolic equations*, Proc. Roy. Soc. Edinburgh 98A, 1984, pp. 193–202.

[24] LeMesurier, B., Papanicolaou, G., Sulem, C., and Sulem, P.-L., *The focusing singularity of the nonlinear Schrödinger equation*, in *Directions in Partial Differential Equations*, M. Crandall et al. eds., Academic Press, 1987, pp. 159–201.

[25] LeMesurier, B., Papanicolaou, G., Sulem, C., and Sulem, P.-L., *The focusing singularity of the cubic Schrödinger equation*, Phys. Rev. A34, 1986, pp 1200–1210.

[26] Mueller, C.E., and Weissler, F.B., *Single point blowup for a general semilinear heat equation*, Indiana Univ. Math. J. 34, 1985, pp. 881–913.

[27] Sulem, P.-L., and Sulem, C., and Patera, A., *Numerical simulation of singular solutions to the two-dimensional cubic Schrödinger equation*, Comm. Pure Appl. Math. 37, 1984, pp. 755–778.

Received January, 1988.

Forthcoming Articles

V. Isakov, On Uniqueness of Recovery of a Discontinuous Conductivity Coefficient

D. G. Schaeffer and E. B. Pitman, Ill-Posedness in Three-Dimensional Plastic Flow

T. Kato and G. Ponce, Commutator Estimates and the Euler and Navier-Stokes Equations

W.-P. Wang, Multiple Impulse Solutions to McKean's Caricature of the Nerve Equation. II. Stability

I. Daubechies, Orthonormal Bases of Compactly Supported Wavelets

A. Bahri and P. L. Lions, Morse Index of Some Min-Max Critical Points. I. Application to Multiplicity Results

J. Hong, On Connectionist Models